

PERFORMANCE EVALUATION OF GAGG+ AND TUNGSTEN CARBIDE BLADES IN AN X-RAY PINHOLE CAMERA

S. Burholt*¹, L. Bobb, N. Vitoratou, Diamond Light Source, Didcot, UK

Abstract

At Diamond Light Source two X-ray pinhole cameras are used to measure the transverse profile of the 3 GeV electron beam. The current pinhole assembly is formed using tungsten blades with chemically etched shims to produce a 25 μm x 25 μm aperture and the imager incorporates a 0.2 mm LuAG:Ce scintillator. Tungsten carbide is a machinable high-Z material which at millimetre thicknesses is opaque to X-rays. With a slight change in pinhole design, similar to that already in place at the ESRF, tungsten carbide blades could offer a well-controlled aperture size for the pinhole camera with simpler assembly. Further to this, improvements to the photon yield of scintillators mean that the new scintillator GAGG+ has an almost two-fold increase in yield compared to the current LuAG:Ce scintillator. An evaluation of the tungsten carbide blades and GAGG+ scintillator is presented.

INTRODUCTION

X-ray pinhole cameras are important diagnostic systems used for beam emittance monitoring at synchrotron light sources. Diamond currently uses two X-ray pinhole cameras downstream of two different bending magnets to provide non-invasive transverse beam profile measurements. These two pinhole cameras are referred to as pinhole camera 1 (P1), and pinhole camera 2 (P2). A schematic layout can be seen in Fig. 1. There is another pinhole camera (P3) set up in a similar way to the other pinhole cameras where research and development projects are carried out.

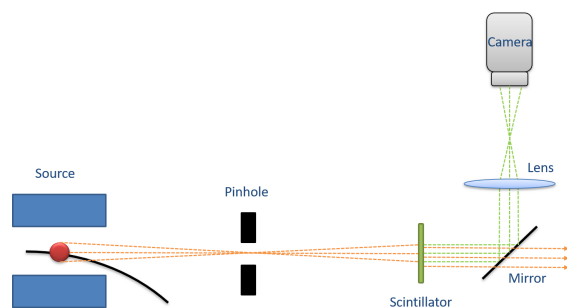


Figure 1: Diamond X-ray pinhole camera layout, including source, pinhole aperture, scintillator, mirror, lens, and camera.

The synchrotron radiation with an energy range of 15 keV to above 60 keV, with a peak around 26 keV, exits vacuum to air through a 1 mm aluminum window. The X-rays then pass through a tungsten pinhole assembly which is formed

of 25 μm x 25 μm apertures [1]. This X-ray beam then interacts with a 0.2 mm thick Lutetium aluminium garnet doped with cerium (LuAG:Ce) scintillator screen and is imaged by a CCD camera (Flea 2), allowing for beam profile measurement and fitting.

The 25 μm pinhole aperture is formed from stacks of 25 mm(h) x 1 mm(v) x 5 mm(d) tungsten blades separated by chemically etched shims of the required thickness [2, 3]. There is one stack vertically and one horizontally so that an aperture of 25 μm in both planes is presented to the X-ray beam. This also forms a 10 mm long tunnel, fully attenuating the beam outside of the aperture. A low flow of nitrogen gas is used to reduce metal oxide growth inside the pinhole assembly.

The spatial resolution of a pinhole camera system can be described by the point spread function (PSF). The PSF is assumed to be constant on relatively long timescales for a given system. For a pinhole camera imaging system the overall PSF may be represented as

$$\sigma_{PSF}^2 = \sigma_{pinhole}^2 + \sigma_{camera}^2 \quad (1)$$

with

$$\sigma_{pinhole}^2 = \sigma_{diffraction}^2 + \sigma_{aperture}^2 \quad (2)$$

and

$$\sigma_{camera}^2 = \sigma_{screen}^2 + \sigma_{lens}^2 + \sigma_{CCD}^2 \quad (3)$$

where the subscripts denote the sources of the PSF contributions [1]. It is well known that there are many contributions to the point spread function. A significant contribution arises from the pinhole aperture [1].

The pinhole aperture material must be opaque to X-rays. A tungsten blade and shim assembly is currently used due to the opacity of tungsten being a high-z material. Shims are required because tungsten is not readily machinable. Therefore the pinhole apertures must be formed using chemically etched shims between the tungsten blades. Due to this the absolute size of the pinhole aperture differs from the shim thickness and is thus unknown. A few factors can cause this discrepancy including; the deformation from cutting or handling the chemically etched shims, misalignment during assembly, and the pressure of the blade-shim-blade assembly. It is also not trivial to measure the pinhole aperture size due to the 5 mm depth of the tungsten blades and three-dimensional structure of the pinhole assembly.

In order to minimise the PSF contribution from the pinhole aperture it is necessary to be able to control the pinhole aperture size and ensure it is matched to the spectrum of the incident synchrotron radiation. Previously machined molybdenum blades were investigated as an alternative to the tungsten/shim design, however the 5 mm molybdenum

* sam.burholt@diamond.ac.uk

blade aperture scans showed a non-linear response indicating insufficient opacity to the X-ray beam [2]. LIGA (X-ray lithography) to produce well-defined apertures in a thin 250 μm gold screen has also been studied, however due to the thickness constraints of the LIGA process, images may require background subtraction. LIGA apertures or slits may be more suitable for monochromatic Fresnel diffractometry and/or interferometry [3].

Tungsten carbide is machinable and provides similar opacity to X-rays as tungsten. At the ESRF tungsten carbide blades using a C-D design have been tested [4]. In this paper, similarly machined tungsten carbide blades are evaluated for the pinhole cameras at Diamond.

From Eq. (3) the overall PSF may be reduced by improving the spatial resolution of the scintillator. Gadolinium aluminium gallium garnet doped with cerium (GAGG+) is a relatively new commercially available scintillator and has been studied for diagnostic applications at other facilities [5–7]. This material has an almost two-fold increase in photon yield (@23 °C) of 40–60 $\times 10^3$ Ph/MeV vs. 25 $\times 10^3$ Ph/MeV for LuAG:Ce which allows for better imaging of the X-ray beam at low current, and enables shorter exposure times thereby reducing the contribution of jitter within images [8]. In this paper the performance of GAGG+ is also evaluated for the X-ray pinhole cameras at Diamond.

TUNGSTEN CARBIDE BLADES

Tungsten carbide blades have been manufactured in the C-D design used at the ESRF [4] with the aperture being formed from an extrusion (D) and void (C) within the stacked blades, rather than with the traditional shim design, or void/flat assembly. The reason for the C-D design is for ease of manufacture: overall it is better to grind larger steps into the tungsten carbide and combining the C-D blades to form the desired aperture size, than trying to grind the 25 μm aperture exactly.

Two tungsten carbide stacks of matching pairs were manufactured with an aperture size of 25 μm . These two pairs were set up within the normal blade stack as shown with a traditional tungsten aperture using 25 μm chemically etched shims. This formed an overall pinhole stack with a 25 μm tungsten-shim-tungsten aperture and a C-D tungsten carbide aperture which allowed for comparative measurements as shown in Fig. 2. Both blades types were manufactured to have overall dimensions of 5 mm in depth, 1 mm in height, and 20 mm in length.

The tungsten carbide blades were manufactured by Midland Carbide [9] and had aperture specification tolerances of $\pm 1 \mu\text{m}$. The blades were manufactured using electro-discharge machining (EDM) to form the overall shape and size then ground and polished to the desired thickness. The stock material was tungsten carbide grade K10, which is the ultra-fine particle size with a material composition of 5.5 % cobalt (Co) and 94.5% tungsten carbide (WC), hardness (HRA) of 92.8, and density of 14.95 g/cm^3 [10].

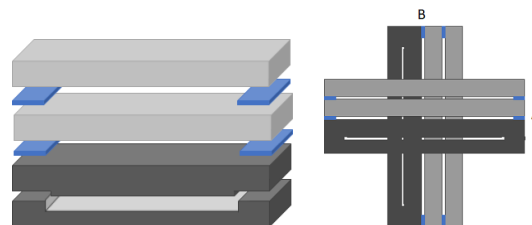


Figure 2: Pinhole blade stack design (left) constructed of tungsten blades (light grey), 25 μm chemically etched shims (blue), and the tungsten carbide C-D design with 25 μm machine gap (dark grey). Stack will be put under pressure when in use to hold all of these as flush as possible. Gaps are not to scale, but to show the C-D design. Total stack formation (right) showing how the apertures are formed from the orthogonal stacks A and B.

Using a back-lit microscope a rough measurement of the pinhole aperture size can be made. With the use of image processing software ImageJ [11] both set of tungsten carbide apertures were measured to be $\approx 35 \mu\text{m}$ in size. This is 10 μm larger than the specification.

TUNGSTEN CARBIDE APERTURE INVESTIGATIONS

Aperture Scans

The pinhole assembly is mounted to translation and rotation stages which allow for remote alignment with the beam. This is required because misalignment can cause reduction in the aperture size for the passing synchrotron radiation. Using the rotation stages the angle of the pinhole aperture relative to the incident beam is varied. During this aperture scan the 2D Gaussian fitted beam sizes (σ_x, σ_y), peak intensity and fit error are recorded via the normalisation of these parameters to their maximum and minimum values as a function of angle.

Higher photon flux through the aperture occurs when the aperture is parallel with the X-ray beam. Thus the measured peak intensity reduces from a maximum value as the angle of the aperture becomes misaligned to the beam.

The horizontal rotation scans of the tungsten and tungsten carbide apertures can be seen in Fig. 3. The horizontal rotation of the blades show the expected increase and decrease in the peak intensity around the aligned position, this can also be seen by the consistent horizontal and vertical beam size measurements throughout the scans.

The vertical aperture scans show a similar response for the peak intensity, as seen in Fig. 4, but the tungsten carbide vertical beam size increases as the system becomes aligned to the X-ray beam, whilst the tungsten blades do not.

This response could be attributed to the larger aperture size of the tungsten carbide assembly when compared to the 25 μm tungsten aperture, as it was found to be 35 μm instead of 25 μm via microscope images. To further show this effect a 50 μm tungsten aperture was tested similarly and

Content from this work may be used under the terms of the CC-BY-4.0 licence © 2023. Any distribution of this work must maintain attribution to the author(s), title of the work, publisher, and DOI

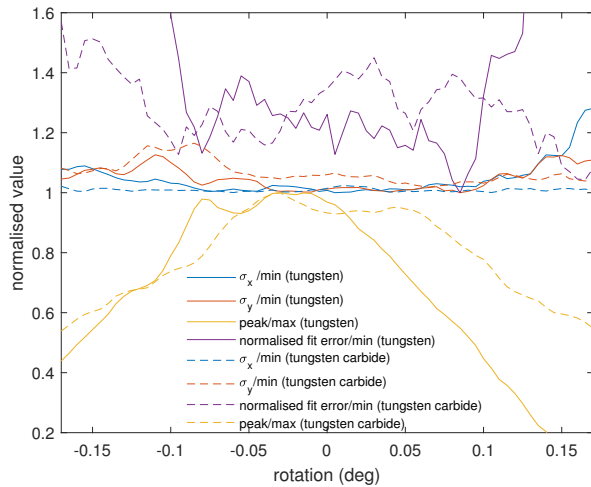


Figure 3: Horizontal rotation scans on pinhole camera 3 of the tungsten aperture (solid lines) and the tungsten carbide aperture (dashed lines).

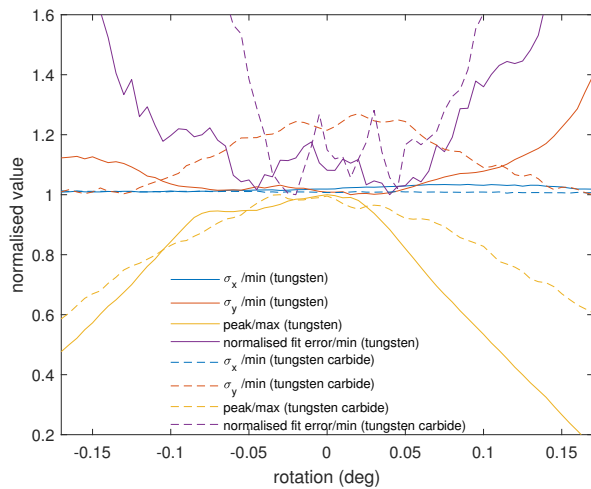


Figure 4: Vertical rotation scans on pinhole camera 3 of the tungsten aperture (solid lines) and the tungsten carbide aperture (dashed lines).

found to have the same response in the fitted vertical beam size (σ_y) and none in the horizontal beam size (σ_x). This shows that the measured beam size of an aperture varies depending on the alignment and size of the aperture due to the PSF contribution. The optimal aperture size for the incident X-ray beam at Diamond is 15 μm [3].

GAGG+ EXPERIMENTS

Modulation Transfer Function Experiments

For these experiments knife-edge images were acquired using a tungsten blade. This blade was placed in front of the scintillator, at a slight angle, to block a portion of the X-ray fan. Knife-edge images are shown in Fig. 5 from which the Edge Spread Function (ESF) is derived. Differentiating

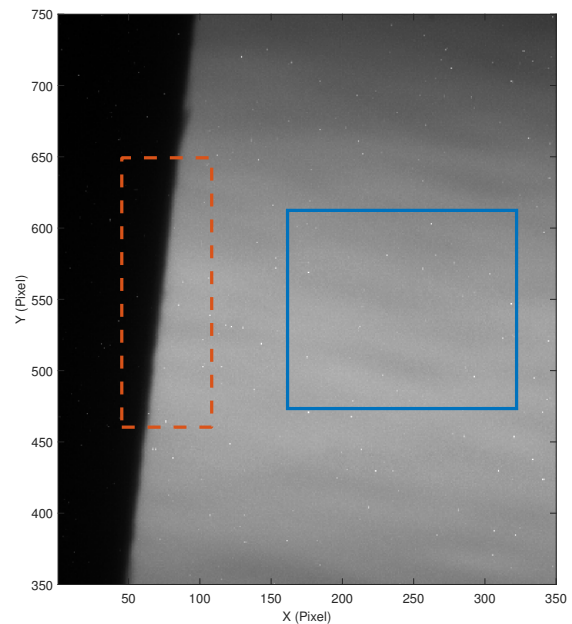
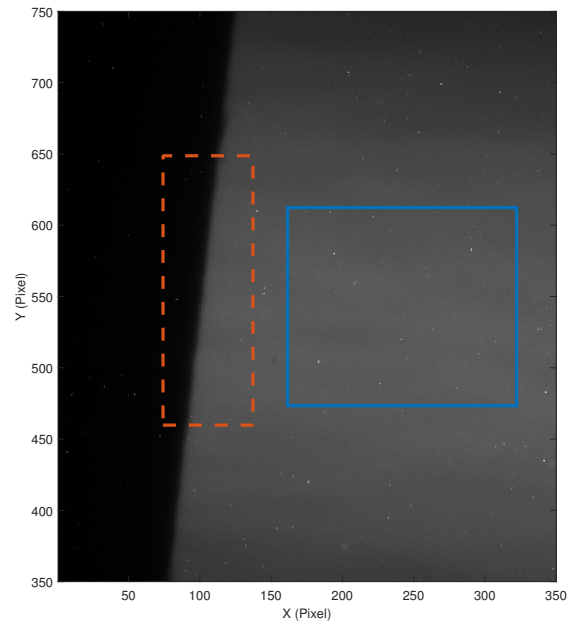


Figure 5: Tungsten blade knife-edge images at the same gain and exposure settings for LuAG:Ce (Top) and GAGG+ (Bottom). ROIs used for knife-edge MTF measurement (dashed orange) and ROIs used for photon yield measurement (solid blue).

the ESF provides the Line Spread Function (LSF) which is analogous to a one-dimensional PSF. Finally the LSF undergoes Fourier Transform to derive the Modulation Transfer Function (MTF) [12–14].

Modulation transfer functions are normally used to investigate the camera lens and camera sensor spatial resolution [13]. The images from the pinhole cameras were taken and processed using QuickMTF which can readily produce the ESF, LSF, and MTF analyses from the region of interest [14].

In order to compare the two scintillators, all aspects of the imaging system (mirror, lens, and camera) remain unchanged. The magnification from the scintillator to the camera sensor is 1.04. The MTF results shown in Table 1 and Fig. 6 have been converted from the image plane (camera sensor) to the object plane (scintillator screen) using the magnification. The MTF10 and MTF50 values in Table 1 have been converted from cycles per pixel to line pairs per mm (lp/mm) using the pixel size of the camera.

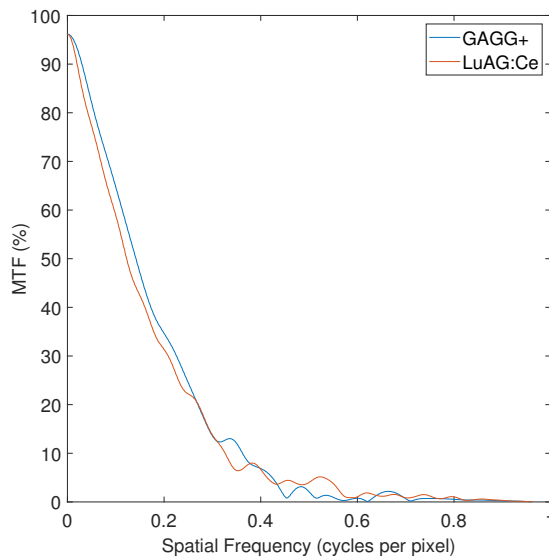


Figure 6: MTF Graph for LuAG:Ce and GAGG+.

Table 1: MTF Results of the Knife-edge Scans of Fig. 6

Value	LuAG:Ce	GAGG+
MTF50 (lp/mm)	27.8	32.0
MTF10 (lp/mm)	70.7	78.6
10 - 90 % rise (pixels)	4.5	3.56

The 10 - 90 % pixel value decreases by one pixel from LuAG:Ce to GAGG+ demonstrating that the edge is sharper. GAGG+ has a slightly increased spatial resolution than LuAG:Ce when referring to the MTF10 and MTF50 values in Table 1, however this increase can be seen to be marginal when compared in Fig. 6. Overall Fig. 6 shows that LuAG:Ce and GAGG+ have similar spatial resolutions.

Photon Yield

A comparison of the photon yield from LuAG:Ce and GAGG+ was undertaken using the ROIs indicated in Fig. 5.

The spectral distribution of the emitted synchrotron radiation was consistent for all studies. The intensity per pixel within these ROIs can be seen in Table 2. This shows an increase in the photon yield of 78 % between the current scintillator LuAG:Ce and the new material GAGG+. These results are also in good agreement with the photon yield specifications for the scintillators which predicted a two-fold increase of GAGG+ compared to LuAG:Ce [8].

Table 2: Intensity Results of a ROI of the Knife-edge Images of LuAG:Ce and GAGG+

	LuAG:Ce	GAGG+
Total Intensity (<i>a.u</i>)	6.04×10^6	1.07×10^7
Pixels in ROI	68769	68769
Intensity per pixel (<i>a.u</i>)	88	157

CONCLUSIONS

This paper investigates whether the use of the new GAGG+ scintillator and tungsten carbide blades could improve the spatial resolution of the X-ray pinhole camera at Diamond Light Source. The microscope images and aperture scans have shown that although specified to 25 μm the new tungsten carbide C-D designed blades have a larger aperture of approximately 35 μm . Aperture scans have shown tungsten carbide is sufficiently opaque to the incident X-ray synchrotron radiation. Although the tungsten carbide aperture shows an increase in vertical beam size during the vertical rotation scan, this can be attributed to its larger aperture size of 35 μm which is less optimal for the given spectrum of synchrotron radiation.

For camera images acquired using the same gain and exposure settings the spatial resolution of GAGG+ and LuAG:Ce has been shown to be almost identical. The expected two-fold increase in photon yield has been largely validated with an 78 % increase in the average intensity per pixel of GAGG+ over LuAG:Ce. This shows that GAGG+ would be a good substitute for LuAG:Ce as it has a higher photon count without any loss in spatial resolution.

REFERENCES

- [1] C. Thomas, G. Rehm, I. Martin, and R. Bartolini, "X-Ray Pinhole Camera Resolution and Emittance Measurement", *Phys. Rev. Spec. Top. Accel Beams.*, vol. 13, no. 2, 2010. doi:10.1103/PhysRevSTAB.13.022805
- [2] L. M. Bobb, A. F. D. Morgan, and G. Rehm, "Performance Evaluation of Molybdenum Blades in an X-ray Pinhole Camera", in *Proc. IBIC'16*, Barcelona, Spain, Sep. 2016, pp. 795-798. doi:10.18429/JACoW-IBIC2016-WEPG63
- [3] N. Vitoratou, L. Bobb, A. Last, and G. Rehm, "X-Ray Pinhole Camera Spatial Resolution Using High Aspect Ratio LIGA Pinhole Apertures", in *Proc. IBIC'22*, Kraków, Poland, Sep. 2022, pp. 71-75. doi:10.18429/JACoW-IBIC2022-MOP18

- [4] F. Ewald, “Emittance diagnostics at ESRF-EBS using the X-ray Pinhole Camera”, presented at the ELETTRA 2.0 Workshop on Optical Diagnostics for Low-Emittance Storage Rings, Mar. 2022. <https://indico.psi.ch/event/12679/contributions/34867/>.
- [5] A. I. Novokshonov *et al.*, “Scintillator Nonproportionality Studies at PITZ”, in *Proc. IBIC’22*, Kraków, Poland, Sep. 2022, pp. 277–280.
doi:10.18429/JACoW-IBIC2022-TUP21
- [6] G. Kube, C. Behrens, C. Gerth, B. Schmidt, W. Lauth, and M. Yan, “Inorganic Scintillators for Particle Beam Profile Diagnostics of Highly Brilliant and Highly Energetic Electron Beams”, in *Proc. IPAC’12*, New Orleans, LA, USA, May 2012, paper WEOAA02, pp. 2119–2121.
- [7] Ch. Wiebers, M. Holz, G. Kube, D. Noelle, G. Priebe, and H.-Ch. Schroeder, “Scintillating Screen Monitors for Transverse Electron Beam Profile Diagnostics at the European XFEL”, in *Proc. IBIC’13*, Oxford, UK, Sep. 2013, paper WEPF03, pp. 807–810.
- [8] Crytur Company Website, Specific GAGG+ and other materials, <https://www.crytur.cz/materials/gagg/>.
- [9] Midland Carbides Company,
<https://www.midlandcarbides.co.uk/>.
- [10] Midland Carbides Company Grades List,
<https://www.midlandcarbides.co.uk/grade-list>
- [11] ImageJ, <https://imagej.net/ij/>.
- [12] S. Lutz *et al.*, “Scintillator Evaluation for High-Energy X-Ray Diagnostics”, United States, Sep. 2001.
doi:10.2172/790063
- [13] F. Viallefont-Robinet *et al.*, “Comparison of MTF measurements using edge method: towards reference data set”, *Opt. Express*, vol. 26, 2018, pp. 33625-33648.
doi:10.1364/OE.26.033625
- [14] QuickMTF Program, <http://www.quickmtf.com/>.